(Received 10 July 2025, Accepted 10 September 2025, Scheduled 15 January 2026)

A Compact Time-Domain Reflectometry (TDR)-Based Microwave Nondestructive Testing Circuit

Nadine A. Shaaban[1] and Ghassan N. Jawad[1, *]

[1] College of Engineering, University of Information Technology and Communications, Baghdad, Iraq
[2] College of Engineering, University of Baghdad, Baghdad, Iraq

ABSTRACT: This paper proposes a proof-of-concept circuit of a time-domain reflectometry (TDR)-based nondestructive testing (NDT) circuit. The circuit consists of a broadband six-port reflectometer with an end-fire antenna probe. The broadband operation is achieved by a reduced-size six-port reflectometer that uses a special algorithm to extend the frequency of operation beyond the limits between which a normal reflectometer is usually used. In addition, a highly-directive antenna probe is proposed to provide a near-constant gain across the bandwidth of operation. By operating the circuit within the frequency range 2.5–7 GHz, it is used to detect gaps of various widths between the back of a polystyrene sample and a metallic plate. Results show a clear indication of the gaps' existence in addition to a shift that is associated with the gap width. The proposed circuit proves the possibility of implementing the TDR-based microwave NDT system using a low-cost and compact circuit without the need for bulky and expensive vector network analyzers. This paves the road towards utilizing this technology in real-life scenarios.

1. INTRODUCTION

Composite materials find applications in numerous fields such as aerospace, construction, and power generation. However, operation and environmental factors can contribute to creating disbanding and delamination within the areas between various layers of the material [1]. Catastrophic failure might occur if these components were not regularly tested and evaluated in a nondestructive manner.

Across the industry, a considerable number of approaches have been proposed to perform this task based on many factors, and the main factor is the type of the material under test [2–5]. However, when the material under consideration is a dielectric composite, Microwave Nondestructive Testing (MNDT) features significant advantages [6–8]. This is mainly due to the ability of microwave signals to penetrate dielectric layers, interact with defects, and provide valuable evaluation information based on the received reflections.

Among MNDT approaches, the Time Domain Reflectometry (TDR) principle allows the usage of a broadband microwave signal to reveal the internal defects using the time domain analysis [8–10].

Figure 1 illustrates the basic principles of TDR-based MNDT. Contrary to other techniques, analysing the reflection coefficient in the time domain allows distinguishing the various reflections in terms of magnitude and distance from the surface of the sample. However, employing this technique requires the testing system to measure the vector reflection coefficient in the time domain, rather than relying on the phase information of the reflection coefficient only [11]. So far, most researchers investigating the MNDT technique using TDR have relied on the conventional Vector Network Analyzer (VNA) to perform this task [8–14]. Clearly, the high cost and bulky nature of the VNA would significantly limit the applicability of this technique in the real world, no matter how promising the results are. Therefore, realizing a stand-alone reflectometer circuit that features the ability to provide the user with a vector reflection coefficient, in addition to a small size and low cost is a necessity. To employ such a circuit in a TDR scenario, some requirements need to be addressed. The first one is the broadband operation, since the resolution of the detection is directly proportional to the bandwidth of the signal being used to perform the scan [8]. The other requirement is realizing a probe that features high directivity, broad bandwidth, and

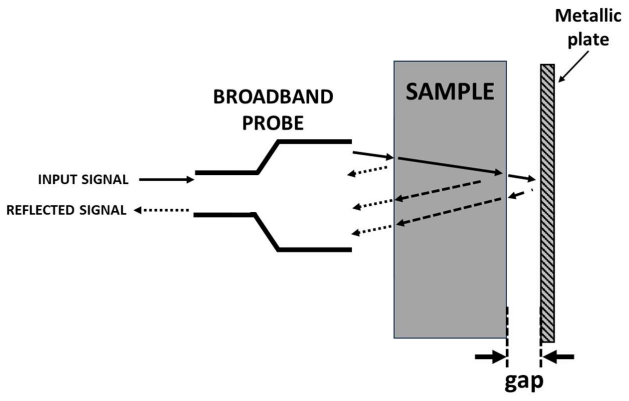

FIGURE 1. Generalized concept of TDR-based MNDT.

* Corresponding author: Ghassan Nihad Jawad (ghassan.jawad@coeng.uobaghdad.edu.iq).

compatibility for integration with the rest of the reflectometer circuit.

Realizing a reflectometer using a heterodyne technology (which is used with conventional VNAs) can provide accurate results over a wide frequency range of operation. However, this technology features significant complexity, which leads to higher cost and larger size [20]. As an alternative, multiport reflectometers are regarded as the most fitting low-cost alternative for measuring vector reflection coefficient over a specific frequency range [13].

The basic concept of a multiport reflectometer (in its most basic forms) has been around since the early 1970s [18]. These designs, which were mainly used for load measurements, rely on arranging a number of couplers and dividers in the path between a microwave source and the Device Under Test (DUT). The internal arrangement of the circuit produces a number of scalar powers to be measured and mathematically converted to the vector reflection coefficient after a number of calibration steps [19]. Over time, the multiport reflectometer design technology evolved by employing different types of couplers and dividers to provide more accurate results, wider bandwidths, and smaller sizes. Moreover, calibration steps have been studied and optimized to realize the aforementioned qualities [20–22]. The improved performance of such circuits has encouraged many researchers to delve into utilizing six port reflectometers for Non-destructive Testing and inspection [23–26]. However, despite the promising results, these designs featured limited bandwidth, which hindered considering the time-domain reflectometry as a potential application of such systems.

In [27], a six-port reflectometer with an extended bandwidth has been proposed, where a special algorithm was employed to extend the bandwidth of the reflectometer to work in frequencies beyond the range at which normal operation occurs with an acceptable level of accuracy. In this paper, a microwave TDR-based NDT circuit is proposed by integrating a broadband antenna probe within the same reflectometer circuit reported in [27] to prove the possibility of achieving broadband TDR-based microwave NDT operation without the need for a VNA.

2. PROPOSED DESIGN

The main goal of the proposed design is to realize a circuit that is able to yield the phasor reflection coefficient (Γ) over a wide frequency range in order to accommodate the requirements of the TDR approach. To achieve this, a six-port reflectometer is used alongside an antenna probe that operates within the same frequency range, as shown in Fig. 2.

The proposed circuit consists of two main components, namely a Six-Port Reflectometer (SPR) and an antenna probe; both are to be discussed in detail in this section.

2.1. SPR Circuit

The reflectometer used in this design consists of six ports, as shown in the diagram in Fig. 3. Here, port 6 is used as an input port and is connected to a sweep microwave generator, where the input signal a_6 is split into five output signals at ports 1, 2, 3, 4, and 5 with various phases and amplitudes. For a normal

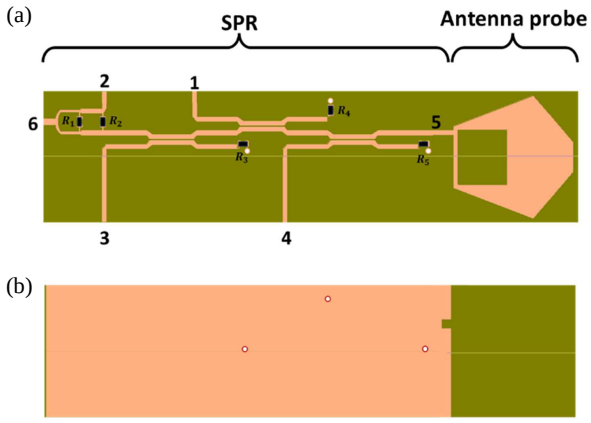

FIGURE 2. Layout of the proposed circuit designed using microstrip technology. (a) Front side, (b) back side.

reflectometer operation, port 5 is usually connected to the DUT. In this work, however, it is connected to the antenna probe. The remaining four ports, namely ports 1, 2, 3, and 4, are connected to matched power detectors that are used to measure the scalar power that reaches each port.

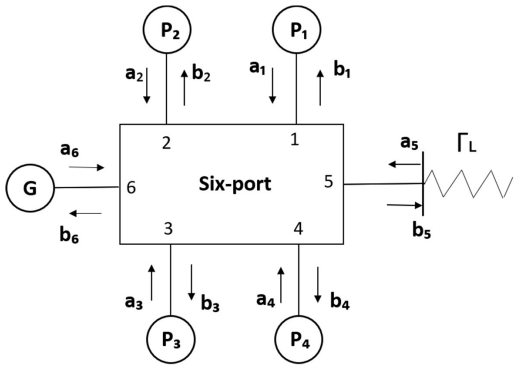

FIGURE 3. Generic block diagram of an SPR.

The estimation of the vector reflection coefficient relies on a calibration procedure which, in this case, involves a couple of loads with known reflection response to be connected and measured. The reflected waves at each port (b_i) is related to the incident and reflected waves to and from the DUT ($b_5 \equiv b$ and $a_5 \equiv a$, respectively) by [30].

$$b = A_i a + B_i b \quad i = 1, 2, 3, \text{ and } 4 \tag{1}$$

where A_i and B_i are complex quantities that rely on the inverse of the matrix equation, which can be determined from the circuit's scattering parameters. Since the detected power at each port is proportional to the magnitude of the corresponding wave squared,

$$P = |b_i|^2 = |A_i a + B_i b|^2 = |b|^2 |A_i|^2 |\Gamma - Q_i|^2 \tag{2}$$

where $\Gamma = \frac{a}{b}$ is the vector reflection coefficient of the DUT, and $Q_i = -B_i/A_i$ is a complex constant at port i (where $i = 1, 2, 3$, and 4). Normalizing the detected power P_i by a reference power (taken here at port 2) yields

$$P = \frac{P_i}{P_i} = C_i |\Gamma - Q_i|^2 \quad i = 1, 3, \text{ and } 4. \tag{3}$$

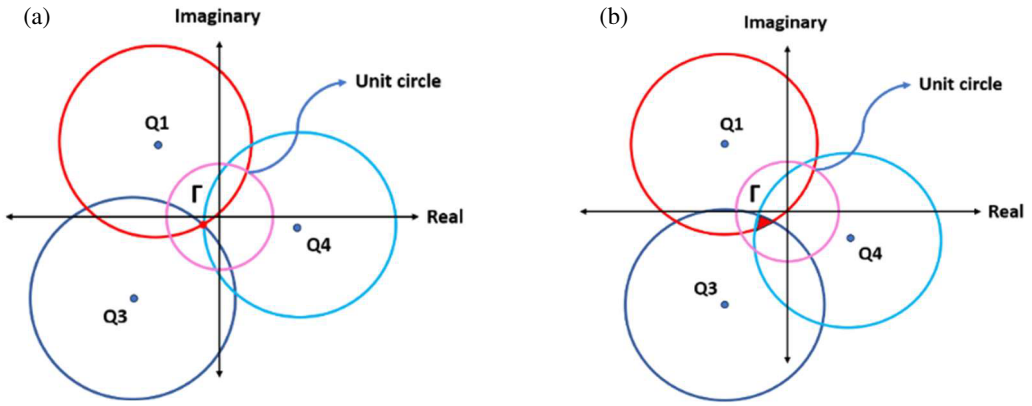

FIGURE 4. Intersected circles resulted from power measurements in an SPR. (a) Ideal case, (b) practical case.

where $C_i = |\frac{A_i}{B_2}|^2$ are real quantities and referred to as the *calibration constants*. These constants can be obtained through a calibration process, where the DUT is replaced by loads with a known reflection coefficient over the desired frequency range of operation. By inspecting (3), it can be deduced that it represents three circles (with respect to the powers measured at ports 1, 3, and 4) in the complex Γ plane, where Q_i represent the centers, and $r_i = \sqrt{C_i/P_i}$ represent the radii.

To implement the SPR illustrated in Fig. 3, it is required to use a 3 dB-power divider at the input of the circuit, where one of its outputs provides the reference power reading (port 2), and the other output feeds three consecutive directional couplers with the coupled arms connected to ports 1, 3, and 4. The output of the last directional coupler feeds the antenna probe. The circuit shown in Fig. 2 represents a compact microstrip SPR with an attached antenna probe designed using a Wilkinson power divider and three edge-coupled directional couplers.

Ideally, the aforementioned circles intersect at a single point within the unit circle for passive loads at the design frequency of the directional couplers and power divider, as illustrated in Fig. 4(a). Ideally, this goal can be achieved at a single frequency point at which the power divider and directional couplers operate. However, to maintain this condition (i.e., the single intersection of the circles), a multistage approach can be used for the divider and couplers to widen the frequency range of operation.

The designed Wilkinson power divider in the proposed system is a 3-dB two-section divider operating from 1 to 6 GHz. The divider includes two sections with two SMD-type isolation resistors ($R_1 = 100\,\Omega$ and $R_2 = 200\,\Omega$). The dimensions of the component have been found after following the approach reported in [28], taking into consideration the FR-4 substrate used for the rest of the reflectometer and antenna probe [27, 31]. The performance of the realized power divider has been verified to show an isolation between its two output ports of more than 10 dB from 1.5 GHz to 9 GHz [27].

As for the required broadband directional coupler, a 16 dB coupler has been designed based on the standard multi-section even-odd mode analysis for microstrip coupled line directional coupler [29]. After choosing the center frequency to be 3 GHz, it was found that the ratio between coupling and isolation is nearly unity from 1 GHz to about 5.5 GHz [27]. Keeping this ratio close to such a value is critical for keeping the Q points near the unit circle and maintain a single intersection of the three circles [21]. Therefore, operating the system within the intended frequency range will render the circles' intersection to form a quasi-triangle, where an estimation of the value of Γ is made from the center of its area, as shown in Fig. 4(b). It is worthwhile to note that the deviation of the intersection points from each other increases for frequencies higher or lower than the design frequency, which increases the probability of erroneous estimation of Γ. For this reason, most reported reflectometers of this type have limited bandwidth to accommodate this condition. However, in [27], an improved approach has been reported which enhances the bandwidth by introducing an algorithm that provides an estimation for the vector reflection coefficient based on analyzing the crossing points of the circles inside (and around) the unit circle. This algorithm aims to enhance the estimation of Γ by processing the intersection points of the circles resulted from the three power measurements, and it can be summarized as follows [27]:

1. The Q-points are obtained and split into real and imaginary parts during the calibration process.
2. The radii of the three circles are determined from measuring the powers at ports 1, 3, and 4.
3. The crossing-points between every two circles (six in total) are found, and the Euclidean distance between any two intersections is obtained.
4. The calculated distances form eight possible triangles. It was found that the centroid of the triangle with the smallest perimeter is the closest point to the correct reflection coefficient.

2.2. Antenna Probe

A probe can be integrated within a reflectometer circuit. In addition, the probe has to feature a small size with an end-fire radiation pattern that is directed towards the forward direction with minimal side lobes. Due to the application of the TDR approach, the gain of the antenna has to be maintained within the same bandwidth of operation of the reflectometer.

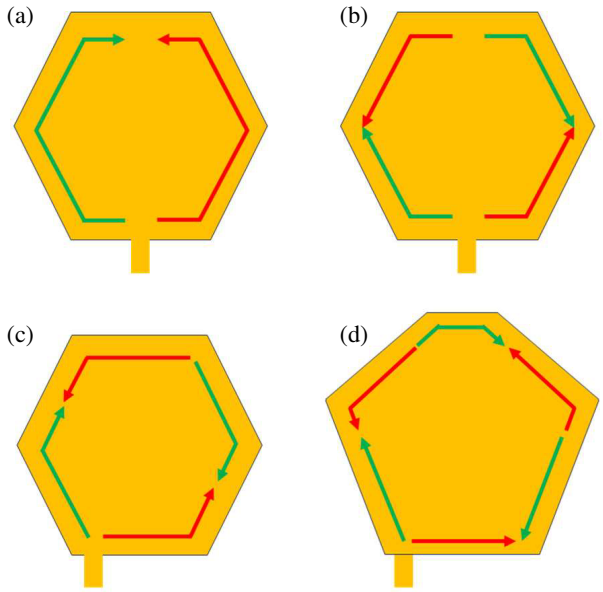

FIGURE 5. Illustration of the hexagonal patch antenna current distribution in (a) the first mode, (b) second mode, (c) second mode with shifted feed, and (d) second mode with shifted feed and optimized sides' lengths.

These challenges have been addressed by designing a hexagonal microstrip antenna with enhanced bandwidth [31, 32]. The design of the antenna is based on modifying the second mode of operation for the basic hexagonal antenna. Figs. 5(a) and 5(b) illustrate the current distribution of the antenna for the first and second modes of operation, respectively, when the feedline is connected to the centre of the bottom side of the hexagon. It is known that the first mode of operation results in an omnidirectional radiation pattern, which does not fulfill the need for the considered operation. The second mode, however, results in two beams directed two upper sides of the hexagonal patch parallel to its plane. To achieve a single beam, the feedline of the patch is shifted towards the edge of the lower side of the patch to modify the current distribution to be as illustrated in Fig. 5(c). Further improvement is achieved in terms of gain and impedance bandwidth when the sides' lengths are optimized, as shown in Fig. 5(d). Impedance matching bandwidth can also be enhanced by exfoliating a rectangular-shaped area in the patch and on the back of the feedline. The final antenna probe with its dimensions is shown in Fig. 6 when it is designed using a 0.8 mm-thick FR-4 substrate. The total size of the antenna is ($50 \times 50\,\text{mm}^2$). Full-wave electromagnetic simulation reveals the current distribution and radiation pattern shown in Fig. 7, at $f = 4.5\,\text{GHz}$.

As illustrated earlier, the gain of the antenna probe has to be maintained (in both the E- and H-planes) within the frequency range of operation. Simulation results show that the designed antenna maintains the maximum gain (amplitude of the main beam) between 4.5 and 5.5 dBi within the frequency range of interest. Moreover, the direction of the main beam should be kept directly in front of the circuit, i.e., at $\theta = 90^\circ$ and $\phi = 0^\circ$. As shown in Fig. 8, the direction of the main beam is with $\pm 20^\circ$ from these ideal values across the considered frequency range.

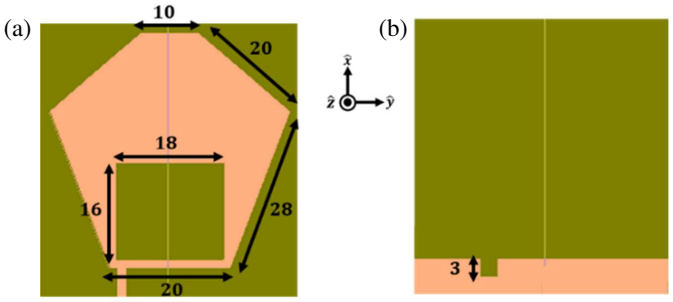

FIGURE 6. Designed antenna probe (all dimensions are in mm). (a) Front, (b) back.

3. RESULTS AND DISCUSSION

To prove the viability of the realized system in a TDR-based NDT scenario, a sample that consists of a single 30 mm-thick layer of polystyrene ($\varepsilon_r = 2.2$) with dimensions of $200 \times 150\,\text{mm}^2$ has been prepared. The sample was then backed by a metallic plate after leaving a gap with a width of (g) that can be changed. The goal of this setup is to test the proposed system for being able to detect the existence of this gap and differentiate between its different widths, which is similar to the process of inspecting material for internal defects, such as delamination. It is well understood that the aforementioned gap has a much smaller size than actual delamination. However, the goal in this work is to prove the possibility of using TDR to detect gaps in metal-backed dielectrics.

An illustration of the experimental setup is shown in Fig. 9, where the reflectometer circuit alongside the antenna probe is placed directly on the surface of the sample.

First, a full-wave electromagnetic simulation (CST MWS) has been used to test the reflectometer algorithm when modelling the arrangement shown in Fig. 9 and running the simulation while changing the gap width (g) between 0 mm and 20 mm with a step of 5 mm. After setting the excitation at the input to the reflectometer circuit (port 6) to be from 2.5 to 7 GHz and collecting the readings at the four ports (1 through 4), the algorithm reported in [27] has been applied to find the reflection coefficient seen at port 5 in the frequency domain. The TDR principle is then applied by finding the reflection coefficient in the time-domain signal for each case of gap width. It is worthwhile to note that the calibration procedure has been done separately by connecting two standards at port 5; one of them is a matched load ($50\,\Omega$), and the other is the antenna probe itself. The results from these calibration steps can be subsequently used for Γ calculations when the SPR and probe are integrated together.

The results shown in Fig. 10 indicate three main peaks; the time step of the first two peaks is fixed for all the gap values, which indicates the reflection originated from the inherent reflection from the antenna itself and the reflection from the surface of the sample. The third peak, on the other hand, shows a clear shift in time as the gap width increases. This is mainly because it originates from the interface between the back of the sample and the space (gap) backed by the metallic plate. From Fig. 10, it can be seen that when the sample (with its metallic back) is removed from the front of the antenna, there is no peak

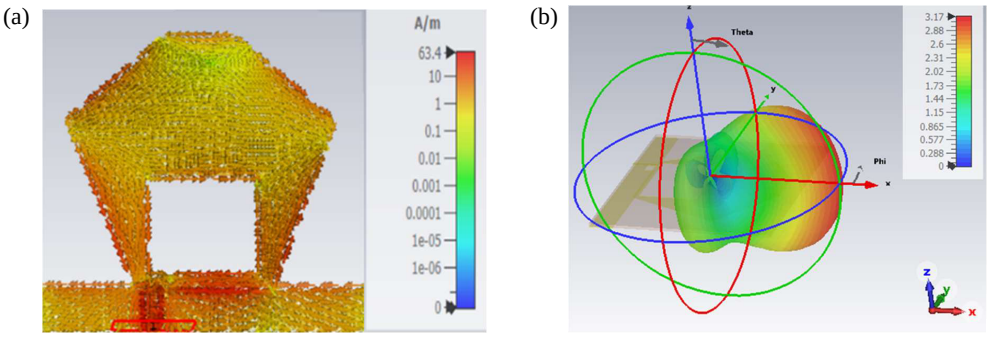

FIGURE 7. Current distribution and radiation pattern, for the designed antenna at $f = 4.5$ GHz. (a) Current distribution, (b) radiation pattern (linear scale).

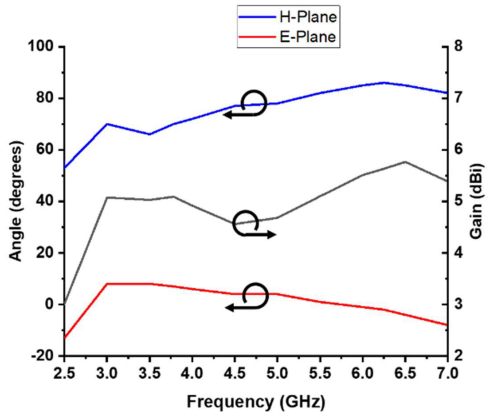

FIGURE 8. Gain and main beam directions in the E- and H-planes for the designed antenna probe.

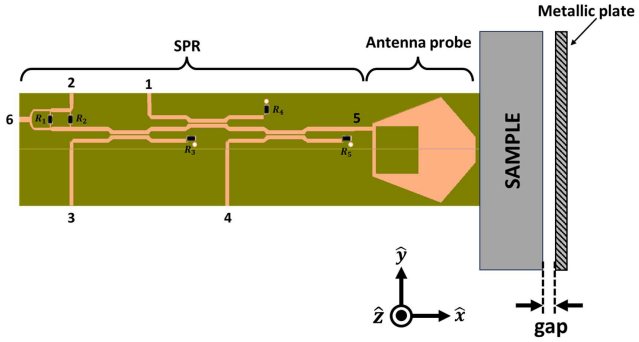

FIGURE 9. Illustration of the experimental setup for gap detection in a metal-backed dielectric sample.

detected at this time step. However, when the sample exists, and the gap gets wider, the peak can be clearly identified. As indicated in the inset of Fig. 10, when the gap width is between 0 mm and 10 mm, the third peak appears at the sixth time step. However, for gap widths of 15 and 20 mm, the peak shifts (delayed) to the next time step (the 7th), which gives an indication of the increased distance the signal has to travel to return to the reflectometer's output port.

It is worth noting here that the resolution of the system is not optimized due to the bandwidth limitation of the SPR and the antenna probe. However, these results can significantly improve as the bandwidth of operation gets wider in accordance with the TDR principles.

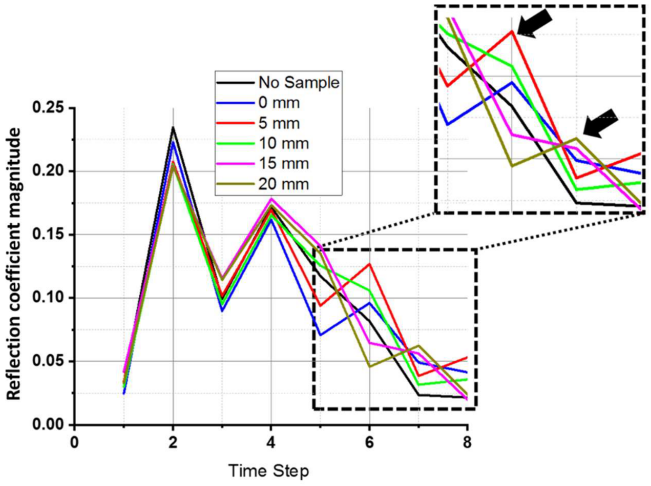

FIGURE 10. Time-domain reflection coefficient for various gap widths resulted from simulating the NDT setup shown in Fig. 9.

The effect of changing the thickness and relative dielectric constant (ε_r) of the metal-backed sample while maintaining a zero gap at its back will be studied next. Simulation results for changing the thickness of the sample are shown in Fig. 11(a).

It can be seen from the results that when setting the thickness of the dielectric sample to 10 mm and 20 mm (while keeping the metallic reflector at its end), there is no significant peak after the second reflection (at time step 4), which indicates that the reflection from the surface of the sample and that from the back reflector have merged together. On the other hand, when the thickness of the sample increases to 30 mm and 40 mm, peaks appear at time steps 6 and 7, respectively. This indicates a distinction in the reflection that can be detected by the system when the reflection from the back reflector is delayed due to the increased thickness.

On the other hand, in Fig. 1(b), the thickness of the sample is kept to 30 mm, while the relative dielectric constant is changed to 2, 4, and 6. From this simulation, the results show that the third reflection peak (which is associated with the back reflector) is shifted from time step 6 to time step 8 when ε_r is changed from 2 to 4, respectively. Moreover, the third reflection peak is shifted further to time step 10 when ε_r is set to 6. This shift indicates more delay in the signal reflected back to the antenna as the phase velocity (ν_p) is decreased due to the increased relative dielectric constant (since $\nu_p = \frac{3\times10^8}{\sqrt{\varepsilon_r}}$).

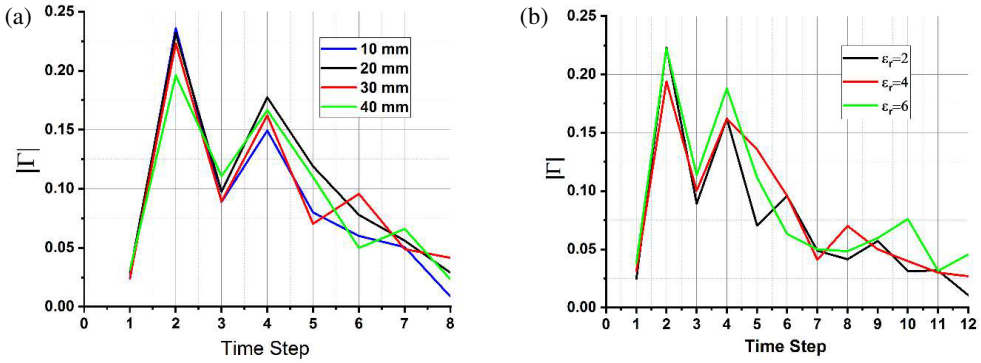

FIGURE 11. Simulation results for the proposed system when changing (a) the thickness and (b) the relative dielectric constant of the sample.

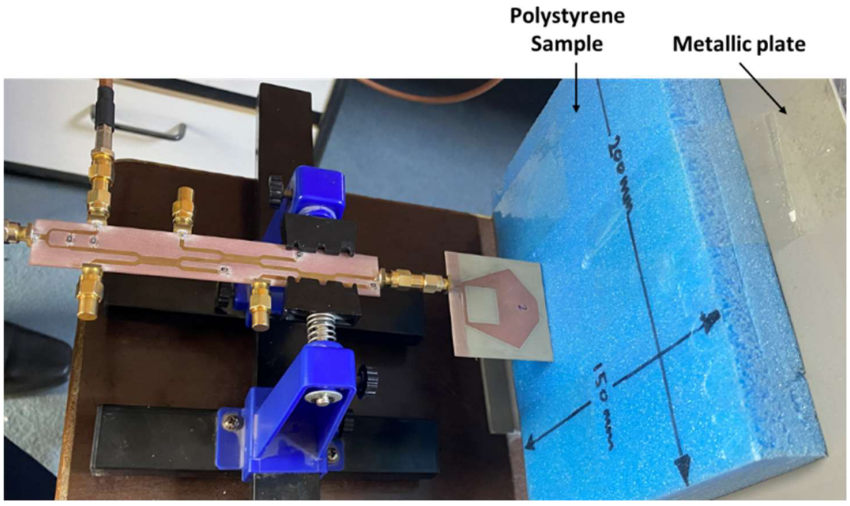

FIGURE 12. Photograph of the experimental setup for the TDR-based NDT scheme using the proposed system.

Finally, the same setup has been implemented to obtain experimental validation of the results for varying the gap between the sample and metallic plate. Fig. 12 shows a photograph of the fabricated SPR with the antenna probe alongside the metal-backed polystyrene sample with a gap width varied as in the previous setup.

After exciting the SPR circuit from a sweep oscillator operating from 2.5 to 7 GHz, the power was measured at each port individually using a microwave power detector that is synchronized with the sweep generator, while terminating all the other ports using matched loads. The power measurement process is repeated for ports 1 through 4 in order to obtain all the powers required to estimate the vector reflection coefficient within the aforementioned frequency range. Next, the vector reflection coefficient was converted to the time domain by applying the Inverse Fast Fourier Transform (IFFT) algorithm to obtain the results shown in Fig. 13 for various gap widths.

The measurement results also indicate two stable peaks at the third- and fifth-time steps, which indicate the reflections from the antenna and the surface of the sample. Other peaks, however, appear for all the cases where the sample and metallic backing exist. For gap widths of 0 mm and 5 mm, the third peak appears at time step 8. On the other hand, for gap widths of 10 mm and 15 mm, the peak appears at time step 10.

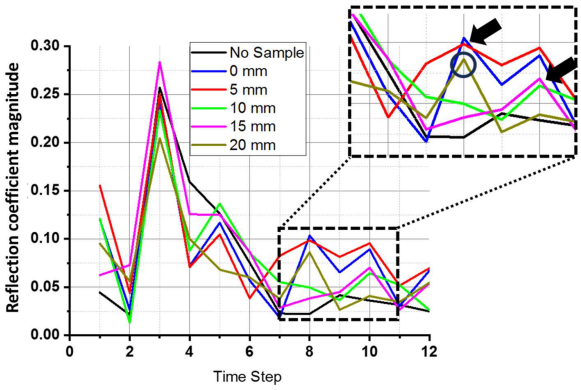

FIGURE 13. Time-domain reflection coefficient for various gap widths resulted from measuring the NDT setup shown in Fig. 11.

An abnormality exists when the gap width is 20 mm, where the peak appears at an earlier time step (the eighth), as indicated by the circle in the inset of Fig. 12, which does not indicate the actual distance between the sample and metallic plate. This abnormality is attributed to numerous factors that contribute to limiting the functionality of the proposed system for large gap widths. First, the existence of the side lobes in the fabricated antenna probe is capable of dominating the reflection in some

cases, while the actual signal reflected to the probe through the sample is scattered or attenuated due to the large distance between the sample and back reflector. Moreover, since the measurements have been performed in a less-than-perfect conditions in a normal laboratory room without any signal absorbers, the system is prone to detecting reflected waves from many objects that surround the experimental setup. In order to reduce the factors that would result in the appearance of premature peaks, the design of the antenna probe can be improved to reduce the Side Lobe Level (SLL) in order to reduce the transmission/reflection in any direction except the intended one. Besides, the testing of the prototype can be performed in an echo-free environment to limit the contribution of the surrounding objects to the overall reflection received by the antenna probe.

Excluding the abnormality for the 20 mm-gap case in the measurement, Fig. 14 shows that the overall behaviour of the measured circuit is similar to the simulation results, where the 0 mm, 5 mm, and 10 mm gaps result in a peak at time step 6 (as illustrated in Fig. 10), and the peak shifts to step 7 for gap widths of 15mm and 20 mm. It should be noted here that the slight difference in the time step numbers between simulation and measurement results is attributed to the slight dimensional differences between the simulated and fabricated circuits.

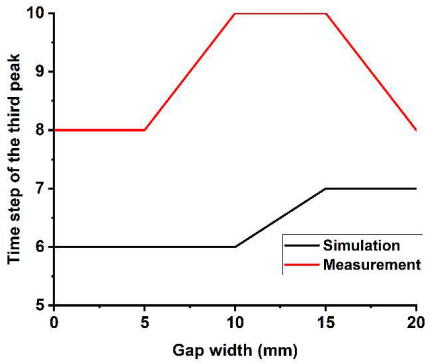

FIGURE 14. Time step of the third reflection peak for both simulation and measurement.

From above, both simulation and measurement results provide an experimental proof-of-principle validation of the proposed system arrangement and the possibility to implement the TDR-based NDT system using a compact and low-cost circuit.

4. CONCLUSIONS

In this paper, a compact and low-cost circuit has been proposed to implement TDR-based microwave nondestructive testing. The proposed circuit consists of a six-port reflectometer connected to a compact antenna probe. The broadband operation for the reflectometer circuit has been achieved by using a multi-section Wilkinson power divider and three multi-section directional couplers arranged to give the best possible performance over the frequency range of interest. The bandwidth of the reflectometer has been further increased by applying a special algorithm to estimate the vector reflection coefficient between the band's edges. The antenna probe has been specifically designed to provide a relatively stable gain in the direction of inspection while considering the compatibility to be integrated with the reflectometer circuit. To prove the validity of the proposed circuit, it has been fabricated using an FR-4 substrate with 0.8 mm thickness and used to detect gaps of various widths between the back of a 30 mm-thick polystyrene sample and a metallic plate. TDR simulation results have shown a clear indication of the existence of the gap, in addition to a shift associated with its width. On the other hand, the existence of the gap and the shift with its width have also been observed in the measured results, with the exception of the 20 mm gap width, which did not reveal the reflection at the correct time step due to the limitation of the antenna probe and high loss of the used sample. The results reported in this paper prove the possibility of using a stand-alone broadband circuit for a TDR-based microwave NDT system instead of relying on bulky and expensive network analysers or narrowband reflectometers. This will pave the way towards realizing compact, portable, and reliable NDT systems that benefit from the TDR features for revealing hidden defects in dielectric materials.

REFERENCES

[1] Akbar, M. F., N. H. M. M. Shrifan, G. N. Jawad, and N. A. M. Isa, "Assessment of delamination under insulation using ridge waveguide," *IEEE Access*, Vol. 10, 36 177–36 187, 2022.

[2] Abdullah, A. A. and H. Çanakcı, "Experimental investigation of crack initiation and growth in concrete slabs placed directly on clayey soil," *Journal of Engineering*, Vol. 28, No. 9, 1–17, Sep. 2022.

[3] Al-Mosawe, M., Y. Al-Shakarchi, and A. A'amal, "Influence of defect in the concrete piles using non-destructive testing," *Journal of Engineering*, Vol. 12, No. 03, 1804–1816, Sep. 2006.

[4] Hadi, N. H. and B. J. Hamood, "Vibration analysis of a composite plate with delamination," *Journal of Engineering*, Vol. 21, No. 02, 144–164, Feb. 2015.

[5] Gao, Y., G. Y. Tian, P. Wang, and H. Wang, "Emissivity correction of eddy current pulsed thermography for rail inspection," in *2016 IEEE Far East NDT New Technology & Application Forum (FENDT)*, 108–112, Nanchang, China, 2016.

[6] Ghasr, M. T., M. J. Horst, M. R. Dvorsky, and R. Zoughi, "Wideband microwave camera for real-time 3-D imaging," *IEEE Transactions on Antennas and Propagation*, Vol. 65, No. 1, 258–268, Jan. 2017.

[7] Siang, T. W., M. F. Akbar, G. N. Jawad, T. S. Yee, and M. I. S. M. Sazali, "A past, present, and prospective review on microwave nondestructive evaluation of composite coatings," *Coatings*, Vol. 11, No. 8, 913, Jul. 2021.

[8] Jawad, G. N. and M. F. Akbar, "IFFT-based microwave nondestructive testing for delamination detection and thickness estimation," *IEEE Access*, Vol. 9, 98 561–98 572, 2021.

[9] Shrifan, N. H. M. M., G. N. Jawad, N. A. M. Isa, and M. F. Akbar, "Microwave nondestructive testing for defect detection in composites based on K-means clustering algorithm," *IEEE Access*, Vol. 9, 4820–4828, 2021.

[10] Akbar, M. F., G. N. Jawad, L. D. Rashid, and R. Sloan, "Nondestructive evaluation of coatings delamination using microwave time domain reflectometry technique," *IEEE Access*, Vol. 8, 114 833–114 841, 2020.

[11] Brinker, K., M. Dvorsky, M. T. A. Qaseer, and R. Zoughi, "Review of advances in microwave and millimetre-wave NDT&E:

Principles and applications," *Philosophical Transactions of the Royal Society A*, Vol. 378, No. 2182, 20190585, 2020.

[12] Xie, Y., X. Yang, P. Su, Y. He, and Y. Qiu, "A microwave time domain reflectometry technique combining the wavelet decomposition analysis and artificial neural network for detection of defects in dielectric structures," *IEEE Transactions on Instrumentation and Measurement*, Vol. 71, 1–11, 2022.

[13] Cataldo, A., E. D. Benedetto, R. Schiavoni, G. Monti, A. Tedesco, A. Masciullo, E. Piuzzi, and L. Tarricone, "Portable microwave reflectometry system for skin sensing," *IEEE Transactions on Electromagnetic Compatibility*, Vol. 71, 1–8, 2022.

[14] Fang, Y., X. Yang, H.-E. Chen, Z. Chen, R. Wang, Y. Li, and S. Xie, "Non-destructive quantitative evaluation of delamination depth and thickness in GFRP using microwave reflectometry," *NDT & E International*, Vol. 144, 103065, 2024.

[15] Arab, H., S. Dufour, E. Moldovan, C. Akyel, and S. O. Tatu, "Accurate and robust CW-LFM radar sensor: Transceiver front-end design and implementation," *IEEE Sensors Journal*, Vol. 19, No. 5, 1943–1950, Mar. 2019.

[16] Ghasr, M. T., D. Pommerenke, J. T. Case, A. McClanahan, A. Aflaki-Beni, M. Abou-Khousa, S. Kharkovsky, K. Guinn, F. D. Paulis, and R. Zoughi, "Rapid rotary scanner and portable coherent wideband q-band transceiver for high-resolution millimeter-wave imaging applications," *IEEE Transactions on Instrumentation and Measurement*, Vol. 60, No. 1, 186–197, 2010.

[17] Engen, G. F., "The six-port reflectometer: An alternative network analyzer," *IEEE Transactions on Microwave Theory and Techniques*, Vol. 25, No. 12, 1075–1080, 1977.

[18] Engen, G. F. and C. A. Hoer, "Application of an arbitrary 6-port junction to power-measurement problems," *IEEE Transactions on Instrumentation and Measurement*, Vol. 21, No. 4, 470–474, 1972.

[19] Hoer, C. A., "Using six-port and eight-port junctions to measure active and passive circuit parameters," U.S. Department of Commerce, National Bureau of Standards, 1975.

[20] Staszek, K., S. Linz, F. Lurz, S. Mann, R. Weigel, and A. Koelpin, "Improved calibration procedure for six-port based precise displacement measurements," in *2016 IEEE Topical Conference on Wireless Sensors and Sensor Networks (WiSNet)*, 60–63, Austin, TX, USA, Mar. 2016.

[21] Ghosh, D. and G. Kumar, "Six-port reflectometer using edge-coupled microstrip couplers," *IEEE Microwave and Wireless Components Letters*, Vol. 27, No. 3, 245–247, Mar. 2017.

[22] Seman, N. and M. E. Bialkowski, "Design of a UWB 6-port reflectometer formed by microstrip-slot couplers for use in a microwave breast cancer detection system," in *2007 IEEE Antennas and Propagation Society International Symposium*, 245–248, Honolulu, HI, USA, 2007.

[23] Feng, P., X. Song, B. Huang, J. Chen, and S. Yan, "An accurate calibration and calculation method of six-port circuit for microfluidic sensing application," *Sensors and Actuators A: Physical*, Vol. 357, 114387, 2023.

[24] Lee, M.-C., "A 20-GHz on-chip six-port reflectometer using simple lumped passive devices and bipolar junction transistors," *International Journal of Engineering and Technology Innovation*, Vol. 3, 01–11, 2024.

[25] Veliz, G. H., C. A. B. Barragán, and F. A. U. Campos, "An efficient 2.4 GHz six-port circuit design to implement a reflectometer," *IEEE Latin America Transactions*, Vol. 21, No. 7, 858–865, Jul. 2023.

[26] Veliz, G. H., F. A. U. Campos, and C. A. B. Barragán, "An alternative design of a compact and portable six-port reflectometer for 2.4 GHz reflection coefficient measurements," *IEEE Latin America Transactions*, Vol. 23, No. 3, 251–257, 2025.

[27] Shaaban, N. A. and G. N. Jawad, "Design and implementation of a microstrip six-port reflectometer (SPR) with enhanced bandwidth," *Journal of Engineering*, Vol. 30, No. 07, 125–143, Jul. 2024.

[28] Mishra, B., A. Rahman, S. Shaw, M. Mohd, S. Mondal, and P. P. Sarkar, "Design of an ultra-wideband Wilkinson power divider," in *2014 First International Conference on Automation, Control, Energy and Systems (ACES)*, 1–4, Adisaptagram, India, 2014.

[29] Pozar, D. M., *Microwave Engineering: Theory and Techniques*, John Wiley & Sons, 2021.

[30] Ghannouchi, F. M. and A. Mohammadi, *The Six-port Technique with Microwave and Wireless Applications*, Artech House, 2009.

[31] Sekhar, M. and N. Suman, "CPW fed super-wideband antenna for microwave imaging application," *Progress In Electromagnetics Research C*, Vol. 130, 201–212, 2023.

[32] Garg, R. K. and S. Singhal, "Hexagon-shaped antenna with DGS for band-notched ultra-wideband and V2X applications," *Telecommunications and Radio Engineering*, Vol. 83, No. 6, 67–77, 2024.